

Chiral current regulation and detection of Berry phase in triangular triple quantum dots

Yue Qi(齐月), Yi-Ming Liu(刘一铭), Yuan-Dong Wang(王援东), Jian-Hua Wei(魏建华), and Zhen-Gang Zhu(朱振刚)

Citation: Chin. Phys. B, 2023, 32 (**8**): 087304. DOI: 10.1088/1674-1056/acd36c
Journal homepage: http://cpb.iphy.ac.cn; http://iopscience.iop.org/cpb

What follows is a list of articles you may be interested in

Chiral symmetry protected topological nodal superconducting phase and Majorana Fermi arc

Mei-Ling Lu(卢美玲), Yao Wang(王瑶), He-Zhi Zhang(张鹤之), Hao-Lin Chen(陈昊林), Tian-Yuan Cui(崔天元), and Xi Luo(罗熙)

Chin. Phys. B, 2023, 32 (**2**): 027301. DOI: 10.1088/1674-1056/ac7208

Multi-carrier transport in $ZrTe_5$ film

Fangdong Tang(汤方栋), Peipei Wang(王培培), Peng Wang(王鹏), Yuan Gan(甘远), Le Wang(王乐), Wei Zhang(张威), Liyuan Zhang(张立源)

Chin. Phys. B, 2018, 27 (**8**): 087307. DOI: 10.1088/1674-1056/27/8/087307

Quantum oscillations and nontrivial transport in $(Bi_{0.92}In_{0.08})_2Se_3$

Minhao Zhang(张敏昊), Yan Li(李焱), Fengqi Song(宋凤麒), Xuefeng Wang(王学锋), Rong Zhang(张荣)

Chin. Phys. B, 2017, 26 (**12**): 127305. DOI: 10.1088/1674-1056/26/12/127305

Topological transport in Dirac electronic systems: A concise review

Hua-Ding Song(宋化鼎), Dian Sheng(盛典), An-Qi Wang(王安琦), Jin-Guang Li(李金光), Da-Peng Yu(俞大鹏), Zhi-Min Liao(廖志敏)

Chin. Phys. B, 2017, 26 (**3**): 037301. DOI: 10.1088/1674-1056/26/3/037301

Topological phase in one-dimensional Rashba wire

Sa-Ke Wang(汪萨克), Jun Wang(汪军), Jun-Feng Liu(刘军丰)

Chin. Phys. B, 2016, 25 (**7**): 077305. DOI: 10.1088/1674-1056/25/7/077305

RAPID COMMUNICATION

Chiral current regulation and detection of Berry phase in triangular triple quantum dots

Yue Qi(齐月)[1], Yi-Ming Liu(刘一铭)[1], Yuan-Dong Wang(王援东)[2], Jian-Hua Wei(魏建华)[1,†], and Zhen-Gang Zhu(朱振刚)[2,‡]

[1] *Department of Physics, Renmin University, Beijing* 100876, *China*
[2] *School of Electronic, Electrical and Communication Engineering, University of Chinese Academy of Sciences, Beijing* 100049, *China*

(Received 7 April 2023; revised manuscript received 6 May 2023; accepted manuscript online 9 May 2023)

Based on the hierarchical equations of motion (HEOM) calculation, we theoretically investigate the corresponding control of a triangular triple-quantum-dots (TTQD) ring which is connected to two reservoirs. We initially demonstrate by adding bias voltage and further adjusting the coupling strength between quantum dots, the chiral current induced by bias will go through a transformation of clockwise to counterclockwise direction and an unprecedented effective Hall angle will be triggered. The transformation is very rapid, with a corresponding characteristic time of 80–200 ps. In addition, by adding a magnetic flux to compensate for the chiral current in the original system, we elucidate the relationship between the applied magnetic flux and the Berry phase, which can realize direct measurement of the chiral current and reveal the magnetoelectric coupling relationship.

Keywords: chiral current, Berry phase, quantum dots, quantum computation

PACS: 73.21.La, 11.30.Rd, 64.70.Tg **DOI:** 10.1088/1674-1056/acd36c

1. Introduction

Electricity to operate a low-dimensional magnetic structure has been an experimental and theoretical research topic over the past twenty years. A variety of configurations have been explored for the electric control of magnetism, such as skyrimions and magnetic domain walls.[1–7] Specifically, in metallic and insulating magnets, electric driven magnetic structure is more ingenious to manipulate and produce ultra-low power consumption, so electric control is highly preferred over magnetism for spin structure regulation. The early investigators have opened the way to efficient control of magnetization through charge transport. Zhang *et al*. revealed when the strong current pulse is applied, a skyrmion will rotate its helicity between $\pi/2$ and $-\pi/2$ based on J_1–J_2–J_3 classical Heisenberg model.[8] Subsequently, the inversion of helicity in a skyrmionic bubble by pure electricity has been demonstrated via a nanostructured frustrated magnetic system.[9] Many studies have been performed to take advantage of this property and the skyrmions are widely used to write qubit states, which can be encoded by the helicity degree.[10–12] Nevertheless, despite tremendous progress, the skyrmion size remained on the order of 100 nm and the current pulse-induced helicity rotation showed randomness.

The recent work related to encoding quantum information using the spin states of quantum dots also generated great excitement, as it fulfilled what were then understood to be the key criteria for quantum computation. Therefore in this paper, we focus on the triangular triple-quantum-dots (TTQDs) system, which is considered as a minimal magnetic structure exhibiting topological properties with three local spins S_1, S_2 and S_3, $S_i = (S_{xi}, S_{yi}, S_{zi})$ $(i = 1, 2, 3)$. The parameters of the TTQD system can be controlled effortlessly, including the bias, grid voltage, pulse signal and interaction strength.[13–16] The chirality in TTQDs, expressed in terms of the spin circulation direction, can be reversed under bias which provides a viable approach to quantum information processing, complementary to superconducting qubits.[17–19] The qubit formed by the three spins can protect quantum information from collective noises, and thus it can resist a full set of random charge fluctuations. Moreover, the application of TTQDs to quantum computing enables scalability in large-scale circuits.[20–22] Through simulation calculation, we find that under the external bias, the chiral operator will split the four-fold degenerate ground states to two chiral state pairs: clockwise (CW) and counterclockwise (CCW) chiral states.

2. Methods

Figures 1(a) and 1(b) show the TTQD structure composed of three coupled quantum dots, where QD_2 and QD_3 are coupled to the electron reservoirs L and R, respectively. The coupling strength between QD_2 and QD_3 is described by t, which can be tuned independently of the other coupling, t_0, between QD_1 and QD_2, QD_1 and QD_3 with single occupation on each dot. The dominant of two chiral states can be further ma-

†Corresponding author. E-mail: wjh@ruc.edu.cn
‡Corresponding author. E-mail: zgzhu@ucas.ac.cn

© 2023 Chinese Physical Society and IOP Publishing Ltd

nipulated by the coupling strength t/t_0 between QDs in the Coulomb blockade regime, as shown by the current circulation direction flipping from the CW to the CCW (see Fig. 1(c)). As a result, the two chiral states can be used to encode qubits and fully use electrical control of the TTQDs under an adjustable coupling strength with ultrafast turnover time. In addition, since the chiral current is not easy to be measured directly in the experiment, we propose to compensate for the chiral current by adding magnetic flux in the original system and further obtain the relationship between the effective magnetic flux phase factor and Berry phase.

The Anderson impurity model of TTQDs was used to demonstrate the proposed approach. Figure 1(a) shows that an electron occupies each quantum dot with spin 1/2. The total system Hamiltonian is $H_{\rm T} = H_{\rm dots} + H_{\rm res} + H_{\rm coup}$. Using the hierarchical equations of motion (HEOM) approximation in the Lorentz hybrid function, which has a universal formalism for an arbitrary system Hamiltonian, we proceed from an isolated TTQD and the t–J–χ Hamiltonian can be obtained by perturbing t in $H_{\rm dots}$ (the detailed derivation of the model is shown in Appendix and Refs. [20,23,24]):

$$H_{\rm eff} = -t(1-n)\sum_{jk,s}(\hat{d}^{\dagger}_{js}\hat{d}_{ks} + {\rm H.c.}) + J\sum_{j<k}\left(\hat{S}_j\hat{S}_k - \frac{1}{4}\hat{n}_j\hat{n}_k\right) + \chi\hat{S}_1\cdot(\hat{S}_2\times\hat{S}_3), \quad (1)$$

where n is the average occupancy on each quantum dot.[25–27] J-term is the Heisenberg exchange interaction, where $J = 4t^2/U$. Under the half-filling situation, $n = 1$, the first item disappears. The last item is the chiral term, where $\chi = 24t_{12}t_{13}t_{23}\sin(2\pi\phi/\phi_0)/U^2$, ϕ is the applied magnetic flux, and $\phi_0 = hc/e$ is the flux quantum. According to the Hellman–Feynman theorem,[28] we define the chiral current operator

$$\hat{J}_{\rm c} = -\frac{e}{\hbar}\left\langle\frac{\partial\hat{H}_{\rm dots}}{\partial\phi}\right\rangle = -\frac{e}{\hbar}\frac{\partial F_{\rm dots}}{\partial\phi} = -\frac{24e}{\hbar}\frac{t_{12}t_{13}t_{23}}{U^2}\hat{S}_1\cdot(\hat{S}_2\times\hat{S}_3), \quad (2)$$

where $F_{\rm dots}$ is the free-energy induced by the magnetic field. The coefficient $t_{12}t_{13}t_{23}/U^2$ represents its nonzero contribution to the lowest-order chiral current. We set $t_{12} = t_{31} = t_0$, $t_{23} = t$ by varying t within the TTQDs to flip the chiral states. With external reservoirs, the spin arrangement of TTQD is non-coplanar, and the chiral symmetry is broken. The chiral operator splits the four-fold degenerate ground states to two chiral-state pairs, $|q_{\pm}^{-1/2}\rangle = \frac{1}{\sqrt{3}}(|\uparrow\downarrow\downarrow\rangle + {\rm e}^{\pm\frac{{\rm i}2\pi}{3}}|\downarrow\uparrow\downarrow\rangle + {\rm e}^{\pm\frac{{\rm i}4\pi}{3}}|\downarrow\downarrow\uparrow\rangle)$, corresponding to the different transmission directions between the CW and CCW of electrons (Figs. 1(a)–1(b)). Typically, the two states are used to define $|0\rangle$ and $|1\rangle$ qubits. When $t/t_0 \sim 1$, the intermediate transition state appears in a linear superposition of CW and CCW chiral states.[29] The chiral current $\hat{J}_{\rm c}$ proposed here is obtained by calculating the partial derivative of the magnetic flux of the Hamiltonian of quantum dots, so it is essentially represented as a chiral operator. In essence, it is characterized as the spin gauge field generated by the interaction between three spins $\hat{S}_1\cdot(\hat{S}_2\times\hat{S}_3)$, which has spin quantum effect. When the chiral operator term acts on the chiral states of the system, the two chiral ground states will split. The chiral circulation will be induced within the whole triangular triple quantum dots, and the chiral state of the dominant system will determine the overall chiral current direction. The two states also can be reversed by means of applied magnetic or temperature gradients. For example, other work by our group also involves the regulation of qubits by temperature gradient.

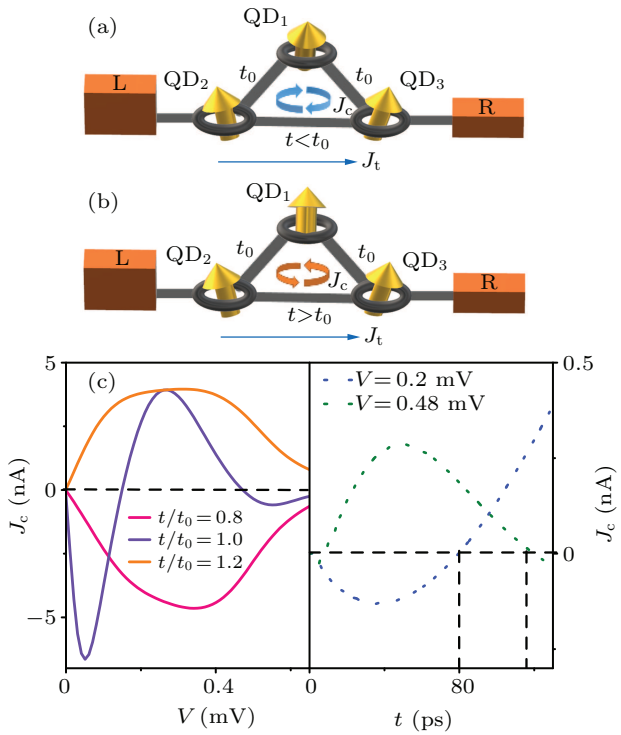


Fig. 1. (a) Schematic diagram of the clockwise chiral current in the TTQD with QD_2 and QD_3 connected to reservoirs L and R, respectively, and (b) the counterclockwise counterpart. (c) Chiral current as a function of bias voltage V under different t/t_0, without magnetic flux. (d) Free evolution time of chiral current $J_{\rm c}$ under bias voltage $V = 0.2$ mV and 0.48 mV. The parameters are (in meV) $\varepsilon = -0.5$, $U = 1.0$, and $t = 0.25$. The system–reservoir coupling strength is $\Delta = 0.025$, and $k_{\rm B}T = 0.05$.

3. Result

For the TTQDs using HEOM method, the paraments were selected as the single occupation energy and Coulomb interaction $\varepsilon = -U/2 = -0.5$ meV.[30–32] During the study, $t_{12} = t_{13} = t_0 = 0.25$ meV was kept unchanged. The couplings between the left (right) electrodes and TTQDs were set to $\Gamma_{\rm L} = \Gamma_{\rm R} = \Delta = 0.025$ meV. Figure 1(c) shows the variation of the chiral states in the TTQD rings, and to further determine the influence of voltage bias on qubits, we calculated the

chiral current J_c as a function of applied bias voltage V for different coupling strengths (t/t_0). For $t/t_0 < 1$ (> 1), the $J_c < 0$ (> 0) and the extremum of J_c decreases as the TTQD system deviates from the C_3 symmetry, which is dominated by CW (CCW) chiral states. The qubit $|0\rangle$ or $|1\rangle$ is only written as a stable state and the chiral state remains localized. For $t/t_0 \approx 1$, we found chiral current J_c oscillations between the two chiral directions, which divide the bias range into CW and CCW regions: the CW region (0 mV $< V <$ 0.15 mV) and the CCW region (0.15 mV $< V <$ 0.45 mV). The flip time of the dominant chiral state occurs promptly, and the typical switching times are 80–200 ps. The time dependence of J_c is plotted in Fig. 1(d). The flipping time of the chiral current direction from CW to CCW is about 80 ps under $V = 0.2$ mV. Meanwhile, the opposite flipping process occurs at $V = 0.48$ mV, corresponding to a characteristic time of 120 ps. The coupling structure of the external reservoirs with the triangular triple quantum dot has been elaborated by wang *et al.*[20] They showed that in TTQD, as the coupling between the spin gauge field and the spin current induces a chiral current at zero magnetic field, the bias induces scalar spin chirality, causing the qubits to be controlled by pure electricity. In further study, we found that both electrical and magnetic control processes can regulate the chiral circulation, and the corresponding regulation between them is approximately linear. In the following work, we still need to carry out further theoretical derivation.

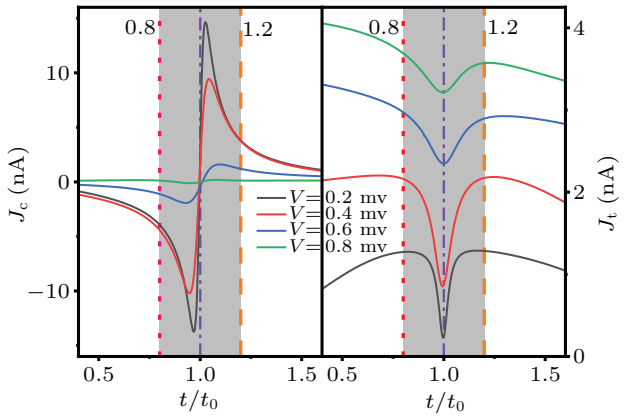


Fig. 2. (a) Chiral current J_c and (b) transport current J_t versus the relative coupling strength t/t_0 at different bias voltages.

Beyond the simple influence of bias voltage, one may add the relative coupling strength to achieve certain design goals related to intrinsic mechanisms. As shown in Fig. 2(a), the chiral current J_c as a function of t/t_0 at different V shows three types of behaviors. For the small relative coupling strength ($t/t_0 < 1$), $J_c < 0$, which corresponds to the CW spin direction, whereas the sign of the chiral current is reversed at large coupling strengths ($t/t_0 > 1$), describing the CCW direction. For the middle coupling strength ($t/t_0 \approx 1$), which is in the intermediate transition state, one finds that J_c sharply jumps under the applied bias voltage, and the extreme values decrease with the increased bias. When $V = 0.2$ mV, J_c can reach about ± 15; however, at $V = 0.8$ mV, $J_c = 0$ nA, which may be related to the severe suppression of J_c with V. Meanwhile, J_t increases with V and for different bias voltages, there exists a valley at $t/t_0 \approx 1$, which is shown in Fig. 2(b).

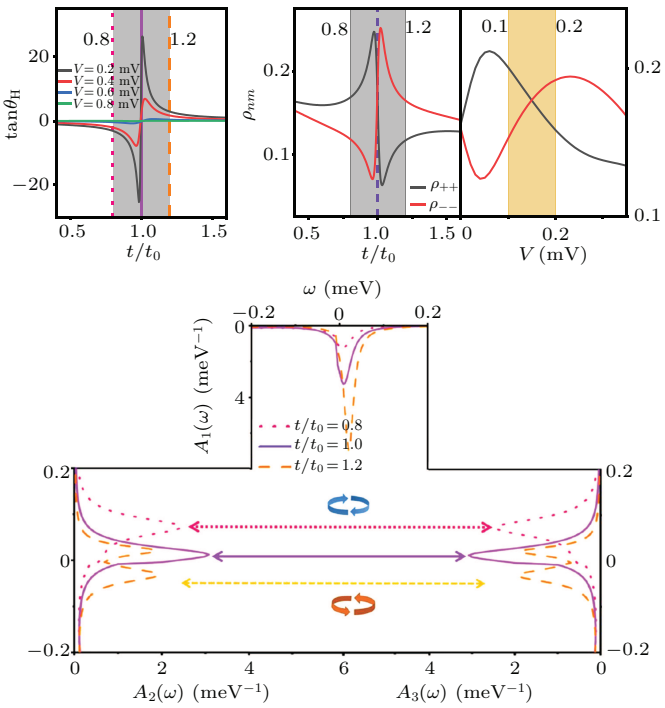


Fig. 3. (a) Effective Hall angle $\tan(\theta_H)$ as a function of relative coupling strength t/t_0 at different bias voltages. (b) t/t_0- and V-dependent populations, ρ_{++} (black curve), and ρ_{--} (red curve) in the three chiral states. (c) Nonequilibrium spectral functions $A_j(\omega) = A_{js}(\omega)$ when $i = 1$, 2, and 3 and $s = \uparrow, \downarrow$ at coupling strengths $t/t_0 = 0.8$, 1.0, and 1.2 without bias voltage ($V = 0$ mV).

To further depict the intrinsic regime, we also investigated the anomalous Hall effect (AHE) in TTQDs.[3] The isolated TTQD ground states are quadruple degenerate, and the adjacent spins have 120° without chirality. By applying a perpendicular magnetic field, this symmetric structure evolves into a nontrivial spin frustration texture. When the electrons jump adiabatically in the TTQDs, an additional Berry (geometric) phase $e^{i\Omega/2}$ can be obtained, which acts as a fictitious magnetic field and tends to dominate the AHE.[34–36] Meanwhile, the chiral current J_c appears and a large effective Hall angle near the turning point emerges. We defined the effective Hall angle, which is analogous to the Hall angle defined by Tatara: the ratio of anomalous Hall conductivity σ_{xy} to the longitudinal conductivity σ_{xx}, the ratio of J_c to J_t, $\tan\alpha_H = \tan(\sigma_{xy}/\sigma_{xx}) \approx \tan\theta_H = \tan(J_c/J_t)$.[37–41] Figure 3(a) shows the effective Hall angle as a function of relative coupling strength t/t_0. For $t/t_0 < 1$ or $t/t_0 > 1$, $\tan\theta_H$ approximately decreases to zero. When $t/t_0 \approx 1$, $\tan\theta_H$ presents a symmetrical jump, and an unprecedented value appears near the flipping point, about $\tan\theta_H = \pm 23$, corresponding to a large effective Hall angle about 87.5°. The maximum value of

the effective Hall angle decays with bias, resulting in a small Hall angle of $\tan\theta_H = \pm 0.1$ under $V = 0.8$ mV.

To explore the physical causes of this phenomenon, we analyzed the reduced density matrix diagonal elements of the two chiral-state populations, i.e., $\rho_{q_{++}}$ and $\rho_{q_{--}}$, by varying the relative coupling strength t/t_0 and bias V, as shown in Fig. 3(b). The sign and magnitude of the difference, $\rho_{q_{++}} - \rho_{q_{--}}$, match well with the observed direction of the calculated chiral current J_c in Figs. 1(c) and 2(a). When $t/t_0 < 1$, the system is in the Coulomb blockade regime, which is responsible for the observed $\rho_{q_{++}} - \rho_{q_{--}} > 0$ and $J_c < 0$. For the case of $t/t_0 > 1$, the sign of $\rho_{q_{++}} - \rho_{q_{--}}$ is symmetry-reversing. In transition states $t/t_0 \approx 1$, at $V = 0.15$ mV, the CW and CCW chiral states are degenerate, $\rho_{q_{++}} - \rho_{q_{--}} = 0$; thus, $J_c = 0$. Figure 3(c) also presents the corresponding nonequilibrium spectral functions $\{A_j(\omega)\}$, with $j = 1$, 2, and 3 of each QD at different coupling strengths for $V = 0$ mV. For $t/t_0 < 1$ and $t/t_0 > 1$, J_t are induced by high excitation peak near $\omega \sim -0.05$ meV and 0.08 meV in QD_2 and QD_3, respectively. For $t/t_0 \approx 1$ at the transition states, each QD peak is near the Fermi level ($\varepsilon_F = 0$), which is the cause that the chiral current changes near the reversal point.

Figure 4 shows the calculated three-dimensional diagram of the chiral current J_c as a function of coupling strength t/t_0 and bias voltage V. The projection diagram of the J_c–t/t_0–V is similar to the "Yin Yang (negative and positive) Fish" diagram of China, and the intermediate transition state is a linear combination between clockwise and counterclockwise chiral states. Therefore, by adjusting the coupling strength t/t_0 between QD_2 and QD_3, we can obtain the clockwise chiral state and counterclockwise chiral state from the 3D stereogram.

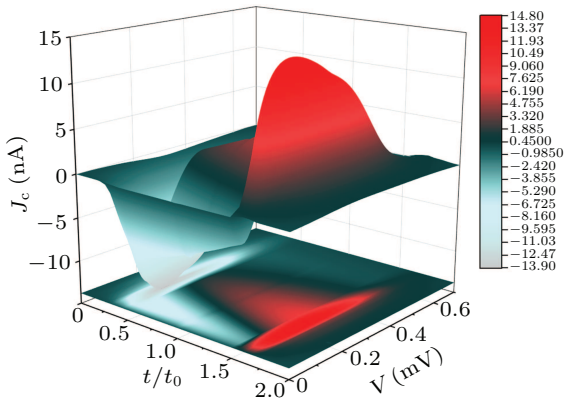


Fig. 4. The 3D image shows J_c as a function of coupling strength t/t_0 and bias voltage V. The filling color depth indicates the strength of J_c.

We further predicted when $t/t_0 < 1$, the distance between QD_2 and QD_3 is relatively far and they form antiferromagnetic spin triplets in the state CW.[42–46] While $t/t_0 > 1$, QD_2 and QD_3 become closer and represent as the effective ferromagnetic interaction induced by relative coupling strength in the state CCW. When $t/t_0 \approx 1$, any two QDs will couple among the TTQDs and form a kink state. We investigated the spin correlation function and the average number of particles occupied to verify the physical model. Figure 5 shows that the $\langle S_i S_j \rangle$ and $\langle n_i \rangle$ as functions of t/t_0 under bias voltage $V = 0$ mV and 0.2 mV. We found that at $t/t_0 < 1$, $\langle S_2 S_3 \rangle > 0$, $\langle S_1 S_2 \rangle = \langle S_1 S_3 \rangle < 0$. And when $t/t_0 \approx 1$, $\langle S_1 S_2 \rangle = \langle S_1 S_3 \rangle = \langle S_2 S_3 \rangle$. This also verifies that there will be a kink point near $t/t_0 \approx 1$. When $t/t_0 > 1$, $\langle S_2 S_3 \rangle < 0$, $\langle S_1 S_2 \rangle = \langle S_1 S_3 \rangle \approx 1$ as QD_1 is decoupled from QD_2 and QD_3. As for the average molecular occupancy, $n_1 + n_2 + n_3 > 3$, indicating that the average molecular occupancy of each quantum dot is generally larger than 1.

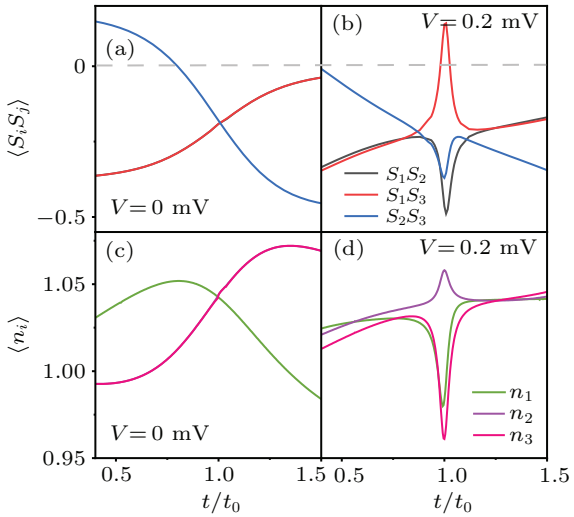


Fig. 5. (a) and (c) The spin correlation function and the average number of particles occupied as functions of t/t_0 under $V = 0$ mV. (b) and (d) are under $V = 0.2$ mV.

The chiral current is an internal effect of TTQDs and is difficult to measure directly in experiments. However, the TTQD system with a topological spin texture generates an equivalent virtual magnetic field corresponding to the net Berry curvature, which can be compensated by the external magnetic flux.[47–49] Our aim was to obtain the effective Berry phase factor in the TTQDs system by the applied magnetic flux.[50] There are two methods to solve this problem and get the relationship between the effective Berry phase factor and the applied magnetic flux in the TTQD system. The schematic of the TTQD connected to two reservoirs using a vertical magnetic field is presented in Fig. 6(a).[51] Here the two reservoirs labeled "L" and "R" are coupled to the TTQDs via the coupling $\Gamma_L = \Gamma_R$, and the bias between the two reservoirs is set as $V = 0.2$ mV. The tunneling coefficients t and t_0 can be tunable with a gate, where we define the parameter $\gamma = t/t_0$ as the relative coupling strength. Here, we use the effective phase factor φ to represent the magnetic flux ϕ, $\varphi = \phi/\phi_0$.

Figure 6(b) shows J_t as a function of γ without φ, and the similar valley structure is found at $\gamma = 1$. This diagram is used as a benchmark for the following two experimental methods.

The first experimental method is to get the scanning image of J_t with γ by adding different magnetic flux phase factors φ, as illustrated in Fig. 6(c). For the case of $\varphi \neq 0$, one can see that the valley depths are reduced by increasing φ, and the magnitude of J_t at $\gamma = 1$ is maximized when the curves change from sharp valleys to approximately linear at $\varphi = 0.14\pi$, which is defined as the effective magnetic flux phase factor φ_c. Figure 6(d) shows the compensation of J_c with γ at different φ. One can find that the fluctuation of J_c gradually decreases by the increase in φ and is approximately compensated to be linear at $\varphi_c = 0.14\pi$.

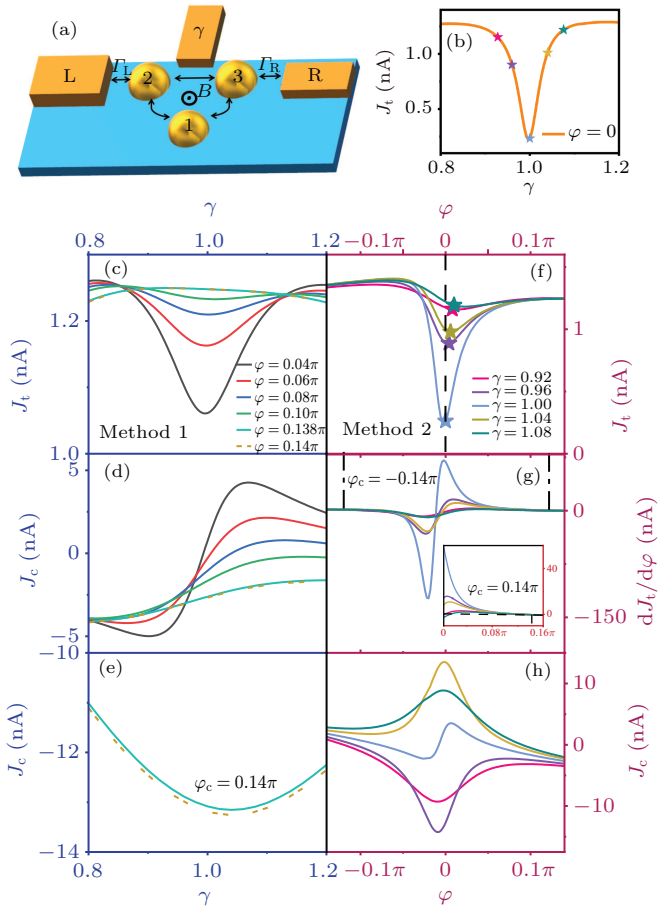


Fig. 6. (a) Schematic diagram of TTQDs with QD_2 and QD_3 connected to reservoirs L and R in a vertical magnetic field with controllable relative coupling strength ($\gamma = t/t_0$). (b) Transport current as a function of relative coupling strength without applied magnetic flux ($\varphi = 0$). (c)–(d) Transport current J_t and chiral current J_c versus relative coupling strength at varying magnetic flux ($\varphi = 0.04\pi$–0.14π). (e) Chiral current J_c as a function of γ under the effective magnetic flux phase factor $\varphi_c = 0.14\pi$ without V. (f)–(h) Transport current J_t, $dJ_t/d\varphi$, and chiral current J_c versus applied magnetic flux φ at different relative coupling strengths ($\gamma = 0.92$–1.08). The inset in (g) shows the magnified section of $\varphi > 0$, indicating the universality of the effective magnetic flux phase factor under different γ, where all curves collapse to a common form.

As shown in Fig. 6(e), in a TTQD without the applied bias ($V = 0$ mV), the circling chiral current J_c is merely induced by φ_c. When $\gamma \approx 1$, J_c reaches the transition state with a maximum of $|J_c| \sim 13$ nA, which is sufficient to reach the magnitude of J_c caused by the bias. As derived by Nagosa *et al.*[33] in the continuum approximation,

$$N_s = \int_A \mathrm{d}x\mathrm{d}y n \cdot \left(\frac{\partial n}{\partial x} \times \frac{\partial n}{\partial y} \right) = \int_A \mathrm{d}x\mathrm{d}y b_z, \tag{3}$$

the phase factor $e^{i\psi} = e^{i(\Omega/2)}$ is given by the flux of the "effective" magnetic field $b_z \cdot \mathrm{d}S = \nabla \times a \cdot \mathrm{d}S$.[52] In our TTQD system, we used the discrete approximation to get the Berry phase, which is equal to $b_z = n_1 \cdot (n_2 \times n_3) = \sigma_1 \cdot (\sigma_2 \times \sigma_3) = 8S_1 \cdot (S_2 \times S_3)$. So

$$|J_c| = \left| \frac{24e}{\hbar} \frac{t_{12}t_{13}t_{23}}{U^2} \hat{S}_1 \cdot (\hat{S}_2 \times \hat{S}_3) \right| = 13, \tag{4}$$

and the parameters are set as $t_{12} = t_{31} = t_{23} = 0.25$ meV, and $U = 1.0$ mV. Plugging these quantities into Eq. (4), we can derive $|\hat{S}_1 \cdot (\hat{S}_2 \times \hat{S}_3)| = 0.153$ corresponding to the Berry phase $\psi_B = (8 \cdot 2\pi)|\hat{S}_1 \cdot (\hat{S}_2 \times \hat{S}_3)| = 1.4\pi$. Another approach is to select five different relative coupling points $\gamma = 0.92$–1.08 and calculate J_t as a function of the applied magnetic flux phase factor φ, as shown in Fig. 6(f). When γ deviates from 1, the corresponding minimum of J_t rises and the valley width decreases. To further apply the magnetic flux in a certain range, we present J_t increasing sharply and less influenced by γ. To determine the effective magnetic flux, figure 6(g) shows $dJ_t/d\varphi$ as a function of φ at different γ. For positive φ, the zero points of $dJ_t/d\varphi$ are $\varphi = 0.14\pi$, which is the same as the first method, and J_c as a function of φ at different γ is shown in Fig. 6(h). For $\gamma > 1$ and $\gamma < 1$, J_c shows peaks with opposite signs induced by the added magnetic flux, resulting in a symmetric line type. Therefore, in the case of a symmetric structure, the compensation of J_c can be realized by only reversing the direction of the magnetic flux.

4. Discussion

The numerical results suggest that building qubits in TTQDs can be manipulated electrically, enabling universal quantum computation that can execute directed quantum state flipping. Their regulation is no longer random compared to skyrmion-based qubits. The time of the switching process is approximately 80 ps, which can realize fast manipulation of spin qubits. In TTQD-based quantum computations, qubit flipping can be regulated by two mechanisms: the external bias and the internal relative coupling strength. Among them, we proposed for the first time that by changing the relative coupling strength between QDs, the chiral-state transformation can be achieved to flip the qubits and there is an unprecedentedly large effective Hall angle at $\gamma = 1$. Furthermore, we elaborate on the feasibility of applying an external magnetic flux to obtain the Berry phase, confirming the chirality of TTQDs for initializing qubits.

The theoretical method we proposed can be easily applied to the experiment, and the specific steps are as follows: Firstly, we easily constructed a TTQD system with QD_2 and QD_3 connected to electrodes. Next, we changed the relative coupling strength between QDs and bias, thus changing the internal chiral states. Finally, Berry phase induced by bias in TTQDs can be obtained by applying magnetic flux, which can further obtain the direction of the chiral current through the conduction current easily measured in the experiment.

At present, the problem of chiral state in TTQDs has not been proposed experimentally. The main reasons are that one such cause is the direct experimental measurement of chiral circulation as impossibly realized in the TTQDs structure, in which one can only get the conduction current. Another related argument is that before our work, there was no theoretical systematic research on the circulation directional overturning problem in TTQDs. Therefore, even though there are many relevant experiments in the TTQDs system, the damping effects caused by the internal circulation have been measured, but no attention has been paid to it, and its intrinsic physical significance has not been realized.

Up to now, QDs have been widely used in quantum computing, and our work can be immediately applied to specific experimental exploration, which can directly relate to the qubit coding by the vector spin chirality and the conduction current. The experimental application is imminent to implement the regulation of novel qubits gate to execute arbitrary quantum algorithms, which has a random-access memory qubit based on TTQDs.

5. Conclusion

By demonstrating the pure electrical control of a magnetic structure, we investigated the regulation of chiral terms in TTQDs. The Berry phase induced by the TTQDs can be obtained by the applied magnetic field, and the direction of the chiral current can be further obtained. By changing the external bias and the structure of the magnetic system itself, we achieved efficient directional flipping from a clockwise chiral state (CW) to a counterclockwise state (CCW). When in transition state, there will generate a large effective Hall angle, which can be adjusted freely by t/t_0. In addition, we also gave two experimental methods for measuring the chiral current. The conversion of the chiral state may lead to innovative applications ranging from magnetoelectric devices to chiral quantum computation.

Acknowledgements

Project supported by the National Natural Science Foundation of China (Grant Nos. 11774418, 11374363, 11674317, 11974348, 11834014, and 21373191), the Strategic Priority Research Program of CAS (Grant Nos. XDB28000000 and XDB33000000), and the Training Program of Major Research Plan of NSFC (Grant No. 92165105). The computational resources have been provided by the Physical Laboratory of High Performance Computing at Renmin University of China.

References

[1] Marrows C and Zeissler K 2021 *Appl. Phys. Lett.* **119** 250502
[2] Xia J, Zhang X, Ezawa M, Tretiakov O A, Hou Z, Wang W, Zhao G, Liu X, Diep H T and Zhou Y 2020 *Appl. Phys. Lett.* **117** 012403
[3] Jin Z, Meng C, Liu T, Chen D, Fan Z, Zeng M, Lu X, Gao X, Qin M and Liu J M 2021 *Phys. Rev. B* **104** 054419
[4] Karnad G, Freimuth F, Martinez E, Conte R L, Gubbiotti G, Schulz T, Senz S, Ocker B, Mokrousov Y and Kläui M 2018 *Phys. Rev. Lett.* **121** 147203
[5] Jin Z, Hu Y, Liu T, *et al.* 2021 arXiv preprint arXiv:2111.00738
[6] Tatara G, Kohno H and Shibata J 2008 *Physics Reports* **468** 213
[7] Nagaosa N and Tokura Y 2013 *Nat. Nanotech.* **8** 899
[8] Zhang X, Xia J, Zhou Y, Liu X, Zhang H and Ezawa M 2017 *Nat. Commun.* **8** 845
[9] Hou Z, Zhang Q, Zhang X, *et al.* 2020 *Adv. Mater.* **32** 1904815
[10] Psaroudaki C and Panagopoulos C 2021 *Phys. Rev. Lett.* **127** 067201
[11] Neto J F and de Souza Silva C C 2022 *Phys. Rev. Lett.* **128** 057001
[12] Xia J, Zhang X, Liu X, Zhou Y and Ezawa M 2022 arXiv preprint arXiv:2204.04589
[13] Saraga D S and Loss D 2003 *Phys. Rev. Lett.* **90** 166803
[14] Weymann I, Bułka B and Barnaś J 2011 *Phys. Rev. B* **83** 195302
[15] Mitchell A K and Logan D E 2010 *Phys. Rev. B* **81** 075126
[16] Liu Y M, Wang Y D and Wei J H 2022 *Chin. Phys. B* **31** 057201
[17] Hsieh C Y, Rene A and Hawrylak P 2012 *Phys. Rev. B* **86** 115312
[18] Kjaergaard M, Schwartz M E, Braumüller J, Krantz P, Wang J I J, Gustavsson S and Oliver W D 2020 *Annual Review of Condensed Matter Physics* **11** 369
[19] Veldhorst M, Hwang J, Yang C, *et al.* 2014 *Nat. Nanotech.* **9** 981
[20] Wang Y, Zhu Z, Wei J and Yan Y 2020 *Europhys. Lett.* **130** 17003
[21] Łuczak J and Bułka B R 2017 *Quantum Information Processing* **16** 1
[22] Gimenez I P, Hsieh C Y, Korkusinski M and Hawrylak P 2009 *Phys. Rev. B* **79** 205311
[23] Li Z, Tong N, Zheng X, Hou D, Wei J, Hu J and Yan Y 2012 *Phys. Rev. Lett.* **109** 266403
[24] Hou D, Wang R, Zheng X, Tong N, Wei J and Yan Y 2014 *Phys. Rev. B* **90** 045141
[25] Scarola V and Sarma S D 2005 *Phys. Rev. A* **71** 032340
[26] MacDonald A H, Girvin S and Yoshioka D T 1988 *Phys. Rev. B* **37** 9753
[27] Cheng Y, Wang Y, Wei J, Zhu Z and Yan Y 2017 *Phys. Rev. B* **95** 155417
[28] Byers N and Yang C 1961 *Phys. Rev. Lett.* **7** 46
[29] Lai C Y, Di Ventra M, Scheibner M and Chien C C 2018 *Europhys. Lett.* **123** 47002
[30] Jin J, Zheng X and Yan Y 2008 *The Journal of Chemical Physics* **128** 234703
[31] Li Z, Cheng Y, Wei J, Zheng X and Yan Y 2018 *Phys. Rev. B* **98** 115133
[32] Chen Z H, Wang Y, Zheng X, Xu R X and Yan Y 2022 *The Journal of Chemical Physics* **157**
[33] Nagaosa N, Sinova J, Onoda S, MacDonald A H and Ong N P 2010 *Rev. Mod. Phys.* **82** 1539
[34] Tatara G and Kawamura H 2002 *J. Phys. Soc. Jpn.* **71** 2613
[35] Fujishiro Y, Kanazawa N, Kurihara R, *et al.* 2021 *Nat. Commun.* **12** 1
[36] Akagi Y and Motome Y 2010 *J. Phys. Soc. Jpn.* **79** 083711
[37] Tatara G 2019 *Physica E* **106** 208
[38] Taguchi K and Tatara G 2009 *Phys. Rev. B* **79** 054423
[39] Xiao D, Chang M C and Niu Q 2010 *Rev. Mod. Phys.* **82** 1959
[40] Onoda S, Sugimoto N and Nagaosa N 2008 *Phys. Rev. B* **77** 165103
[41] Ishizuka H and Nagaosa N 2021 *Phys. Rev. B* **103** 235148
[42] Yao X, Chen J and Dong S 2020 *New J. Phys.* **22** 083032

[43] Huang J and Wang W Z 2018 *Chin. Phys. B* **27** 117303

[44] Xiong Y C, Zhou W H and Zhang J 2017 *Journal of Low Temperature Physics* **187** 298

[45] Tooski S, Ramšak A and Bułka 2016 *Physica E* **75** 345

[46] Bonča J, *et al.* 2008 *Phys. Rev. B* **77** 245112

[47] Zhang S S, Ishizuka H, Zhang H, Halász G B and Batista C D 2020 *Phys. Rev. B* **101** 024420

[48] Koga M, Matsumoto M and Kusunose H 2014 *J. Phys. Soc. Jpn.* **83** 084707

[49] Denisov K 2020 *J. Phys.: Condens. Matter* **32** 415302

[50] Metalidis G and Bruno P 2006 *Phys. Rev. B* **74** 045327

[51] Noiri A, Kawasaki K, Otsuka T, *et al.* 2017 *Semiconductor Science and Technology* **32** 084004

[52] Lee P A 2007 *Handbook of High-Temperature Superconductivity* (Springer) pp. 527–568

[53] Kehrein S K and Mielke A 1996 *Annals of Physics* **252** 1

[54] Feynman R P and Jr F V 1987 *Annals of Physics* **281** 547

[55] Li Z H, Tong N, Zheng X, Hou D, Wei J, Hu J and Yan Y 2009 *Phys. Rev. Lett.* **109** 266403

[56] Ye L Z, Wang X, Hou D, Xu R X, Zheng X and Yan Y 2011 *Wiley Interdisciplinary Reviews Computational Molecular Science* **133** 101106

[57] Cheng Y X, Wang Y D, Wei J H, Luo H G and Lin H Q 2019 *J. Phys.: Condens. Matter* **31** 155302